THESIS FOR THE DEGREE OF LICENTIATE OF ENGINEERING

Laser powder bed fusion processing and heat treatment of Ni-base superalloys: microstructure and properties

Abdul Shaafi Shaikh

Department of Industrial and Materials Science
CHALMERS UNIVERSITY OF TECHNOLOGY
Gothenburg, Sweden 2022

Laser powder bed fusion processing and heat treatment of Ni-base superalloys: microstructure and properties

Abdul Shaafi Shaikh

Technical report no IMS-2022-6

Department of Industrial and Materials Science
Chalmers University of Technology
SE-412 96 Gothenburg
Sweden
Telephone + 46 (0)31-772 1000

Printed by Chalmers Reproservice
Gothenburg, Sweden, 2022.

Laser powder bed fusion processing and heat treatment of Ni-base superalloys: microstructure and properties

ABDUL SHAAFI SHAIKH

Department of Industrial and Materials Science
Chalmers University of Technology

Abstract

Nickel-base superalloys are indispensable materials for the energy and aerospace industries. The additive manufacturing (AM) of these materials by powder bed fusion – laser beam (PBF-LB) presents a valuable opportunity to improve component performance and ease manufacturing and supply chain complexity in these industries. However, only a limited number of Ni-base superalloys are currently available for PBF-LB. This is due to several challenges encountered during PBF-LB processing, including microcracking, post-process cracking, development of an AM-specific microstructure, and lack of heat treatment optimization.

The aim of this thesis study is to develop better understanding of the extent of these issues in different superalloys, their causes, and potential remedies. To understand aspects of processability, the alloy Haynes® 282® was studied to assess its feasibility for manufacture by means of PBF-LB, including susceptibility to cracking. Results showed excellent processibility of Haynes® 282® by PBF-LB, allowing to reach full-density crack-free components over the wide range of energy input, while also being resistant to post-process cracking.

Conventionally manufactured superalloys – cast or wrought – are currently considered as the benchmark in terms of mechanical performance. The microstructure and mechanical performance of PBF-LB processed Haynes® 282® after standard heat treatment was evaluated and compared to its wrought counterpart from the literature. PBF-LB processed Haynes® 282® showed finer grain sizes and discontinuous grain boundary carbides compared to wrought microstructure. Despite excellent room temperature tensile properties, clear anisotropy in high temperature mechanical performance of PBF-LB processed Haynes® 282® was observed, which is proposed to be addressed by heat treatment optimization.

Heat treatment is a critical post processing step for any precipitation strengthened alloy, and this is especially true for PBF-LB processed superalloys. Heat treatments developed for cast or wrought alloys may not be optimal for the same alloys in PBF-LB processed form because PBF-LB processed superalloys have a starting microstructure that is very different from equivalent cast or wrought microstructures. This aspect was studied in detail by evaluation of the as-built microstructure of Inconel 939, a high γ'-fraction superalloy. No γ' precipitates were found in the as-built microstructure, however, η phase was found at inter-dendritic regions. This secondary phase was observed to grow upon ageing, lowering the ductility of the material. This demonstrates the importance of a solution treatment for Inconel 939, regardless of γ' in the as-built condition. Further study also aimed to optimize the ageing heat treatment steps for PBF-LB manufactured Inconel 939. This resulted in a proposed ageing heat treatment which is shorter than the one used for conventional cast Inconel 939, which also produces improved and more isotropic tensile performance. Another aspect of heat treatment in PBF-LB processing is potential contamination of an alloy from the stress relief heat treatment carried out while a part is fused to a dissimilar building platform material. This was addressed in a study on Haynes® 282® built onto a carbon steel building platform. The study showed that no large-scale change in chemical composition occurred, suggesting that steel platforms are suitable for use with Ni-base superalloys.

Keywords: Additive manufacturing; powder bed fusion – laser beam; superalloys; Haynes 282; Inconel 939; heat treatment; microstructure.

Preface

The work presented within this thesis was performed at the Research & Development Department of EOS Metal Materials in Turku, Finland, and at the Department of Industrial and Materials Science, Chalmers University of Technology, Gothenburg, Sweden between June 2019 and December 2021. The work was conducted in the framework of the Center for Additive Manufacturing – Metal (CAM^2), supported by Vinnova, as an industrial PhD project financed by EOS Metal Materials. The research was supervised by Professor Eduard Hryha of the Department of Industrial and Materials Science at Chalmers and Kevin Minet-Lallemand from EOS Metal Materials. Professor Lars Nyborg was the examiner.

List of appended papers

Paper I **Microstructure and mechanical properties of Haynes 282 superalloy produced by laser powder bed fusion**

Abdul Shaafi Shaikh, Fiona Schulz, Kevin Minet-Lallemand, Eduard Hryha

Materials Today Communications 26 (2021) 102038

Paper II **On the effect of building platform material on laser-powder bed fusion of a Ni-base superalloy HAYNES® 282®**

Abdul Shaafi Shaikh, Fiona Schulz, Kevin Minet-Lallemand, Eduard Hryha

Submitted for journal publication

Paper III **On as-built microstructure and necessity of solution treatment in additively manufactured Inconel 939**

Abdul Shaafi Shaikh, Masoud Rashidi, Eduard Hryha, Kevin Minet-Lallemand

Powder Metallurgy (2022)

Paper IV **On the additive manufacturing of Inconel 939 – Analysis of microstructure and re-development of heat treatment**

Abdul Shaafi Shaikh, Kevin Minet-Lallemand, Eduard Hryha

Proceedings of EuroPM2020 Conference, 2020

Contribution to appended papers

In **Paper I**, the author planned the study, performed the experiments, analysed the results and wrote the paper in collaboration with the co-authors.

In **Paper II**, the author planned the study along with the co-authors and supervisors. The author conducted the experiments in collaboration with Fiona Schulz. The author analysed the results and wrote the paper in collaboration with the co-authors.

In **Paper III**, the author planned the study and performed all the experiments, except for TEM analysis, which was performed by Masoud Rashidi. The author analysed the results and wrote the paper in collaboration with the co-authors.

In **Paper IV** the author planned the study in collaboration with supervisors, and conducted the experiments, analysed the results, and wrote the paper in collaboration with the co-authors.

Contents

List of abbreviations

AM	Additive manufacturing
PBF-LB	Powder bed fusion – laser beam
LPBF	Laser powder bed fusion
CAD	Computer aided design
GA	Gas atomization
VIGA	Vacuum inert melting gas atomization
PREP	Plasma rotating electrode process
BD	Building direction
PM	Powder metallurgy
LoF	Lack of fusion
HIP	Hot isostatic pressing
TCP	Topologically close packed
ODS	Oxide dispersion strengthening
HAZ	Heat affected zone
SAC	Strain age cracking
DDC	Ductility dip cracking
ITE	Intermediate temperature embrittlement
SEM	Scanning electron microscope
FEG	Field emission gun
BSE	Backscattered electron
EDX	Energy dispersive X-ray spectroscopy
EBM	Electron beam melting
PBF-EB	Powder bed fusion – electron beam

1. Introduction

Additive manufacturing or 3D printing in general, and laser powder bed fusion (LPBF) in particular, shows great promise as an upcoming manufacturing process for high performance components. Greater design freedom and faster time from design to production are two of the main benefits of LPBF. However, even though LPBF offers the largest material portfolio of metal AM processes, the technology is still severely limited in the number of materials available with which parts can be reliably manufactured. More high temperature materials and Ni-base superalloys in particular, are needed on account of their unique combination of properties.

Extensive research into LPBF of superalloys has shown that there are still number of unsolved technical challenges that restrict the adoption and application of superalloys for LPBF. Many superalloys have been shown to suffer from microcracking during the LPBF process. Cracking during post-process heat treatment has also been encountered particularly for superalloys with higher fractions of strengthening phases. When it has been possible to produce superalloys without defects, the high temperature mechanical performance has been found to be below the level of their conventionally manufactured counterparts. This is thought to be at least partially due to the difference in microstructure, e.g. grain size and texture, compared to cast and wrought superalloys. This difference also necessitates re-evaluation and often re-development of the solution and ageing heat treatments for common superalloys produced by LPBF as a means of raising the mechanical performance to be competitive with conventionally produced materials.

As a result, continued efforts are required to better understand the challenges associated with LPBF processing of Ni-base superalloys and develop strategies to mitigate them.

1.1. Research Objectives

The objective of this research is to evaluate the processability, microstructure and properties of precipitation strengthened Ni-base superalloys by LPBF, with particular attention to the research questions:

RQ 1: What are the main factors determining LPBF processability of weldable and non-weldable precipitation strengthened Ni-base superalloys?

RQ 2: What are the main microstructural differences between conventional and LPBF-processed Ni-base superalloys and their effect on mechanical performance?

RQ 3: What is the optimal post-AM heat treatment for LPBF-produced precipitation-strengthened Ni-base superalloys?

2. Review of the Literature

2.1. AM Fundamentals

Conventional manufacturing often starts with raw material in the form of an ingot or billet, from which material is progressively removed until the shape of the desired component is achieved. This is subtractive manufacturing. Alternatively, the starting shape is progressively deformed to generate desired geometrical features, or otherwise melted down and poured into a mould in the shape of the desired component. In additive manufacturing (AM), however, material is added layer by layer until the required component geometry is formed. Compared to conventional manufacturing, AM has several advantages.

Freedom of design is a chief advantage – designers are not limited by the access of cutting tools, or fixturing and clamping restrictions, and highly complex geometries can be manufactured with internal features or complex curves that would not be possible or economically feasible by conventional methods. Material waste is also reduced compared to machining. In subtractive manufacturing, much material ends up as chips. In AM only the material that is added to the part is consumed, and the rest can (at least in principle) be reused for the next production part. Another major advantage of AM is the reduced need for tooling or moulds. These can be a major limitation in near-net-shape manufacturing processes, such as injection moulding and casting, where a tooling or mould must first be created before any components can be manufactured. Often the production of tooling or moulds is expensive and time consuming. On the other hand, AM allows parts to be manufactured directly from a digital design drawing, thus reducing lead times as well as ancillary costs. A related advantage of AM is customizability. Since no permanent tooling or mould is needed, each manufactured part can be unique in design at no extra cost. It is owing to these advantages that AM has seen an exponential rise in adoption in recent times.

The AM is often referred to colloquially as 3D printing. There are seven different technology families within AM, as defined by the ISO / ASTM 52900:2021 standard [1]. These technologies can be used for many material classes, including metallic materials, polymers, and ceramics. For the purpose of this thesis study, powder bed fusion (PBF) of metallic materials is the technology of relevance.

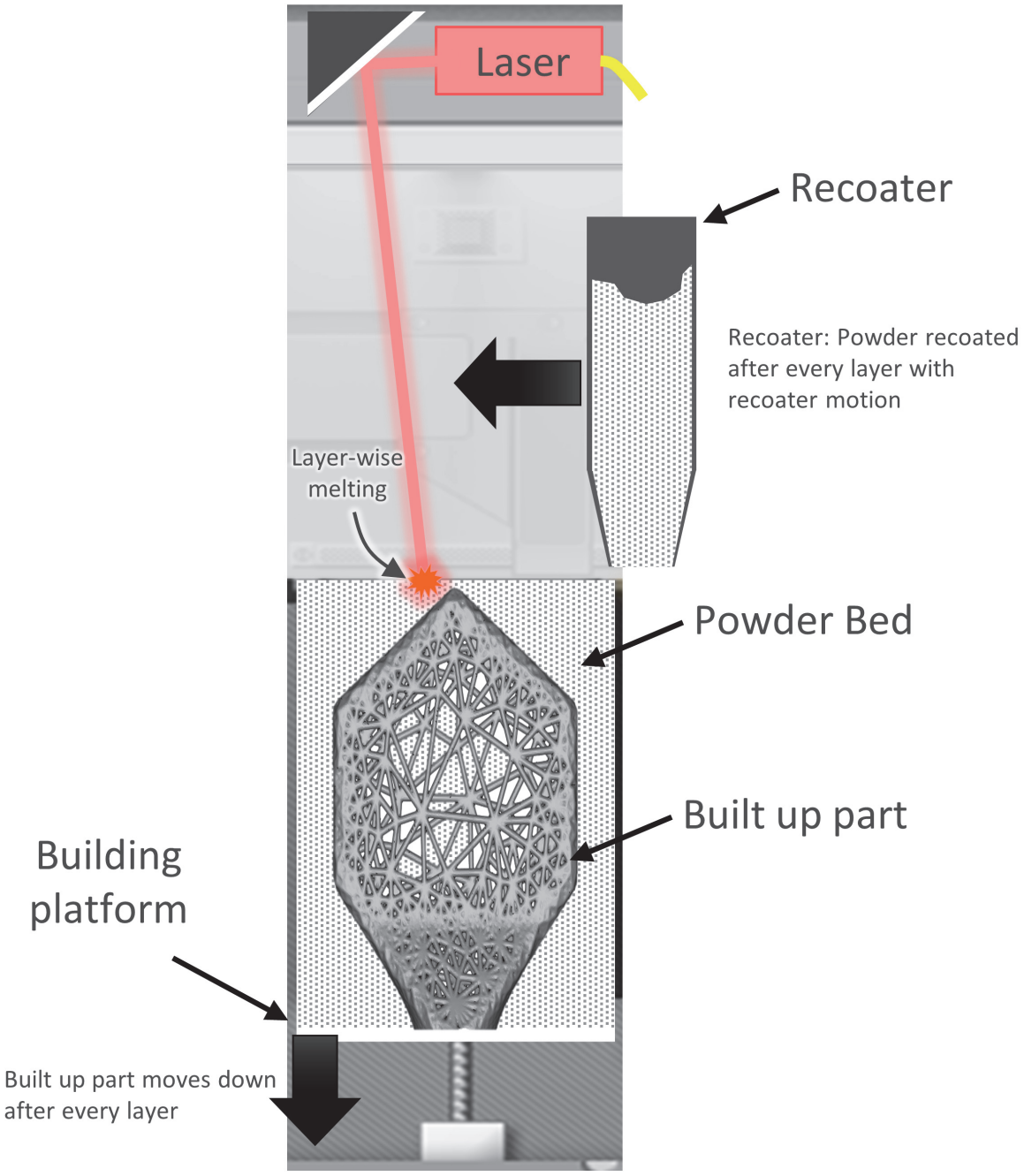

Figure 1: Schematic of a generic LPBF system and its function.

2.1.1. LPBF basics

Laser Powder Bed Fusion (LPBF) is an AM process that involves a bed of fine powder and a heat source in the form of a laser beam. A schematic representation of an LPBF system is shown in Figure 1. The laser is mounted to a scanner unit which allows extremely precise 2-dimensional patterns to be exposed by the laser beam. The laser has enough power to produce melting of the powder and already deposited material. The powder is spread onto a substrate, known as the building platform, in the form of thin layers, usually 20 to 100 µm in height. Meanwhile, the part to be manufactured is prepared in the form of a 3D model using Computer Aided Design (CAD) software. The 3D model is "sliced" into layers corresponding to the layer thickness to be used by the LPBF process. The 2-dimensional profile of each layer is then scanned over by the laser, melting and consolidating the powder as well as fusing it to the building platform. The building platform is lowered by the height of one layer, and another layer of powder is spread on top. This layer is also melted by the laser beam according to the slice from the 3D model, and the process repeats until all layers have been processed. This results in a solid part attached to the building platform within a bed of powder. This part is then separated from the building platform by some sawing process, heat treated, and surface treated if required. Figure 2 shows an example of a completed LPBF build after being lifted out of the powder bed.

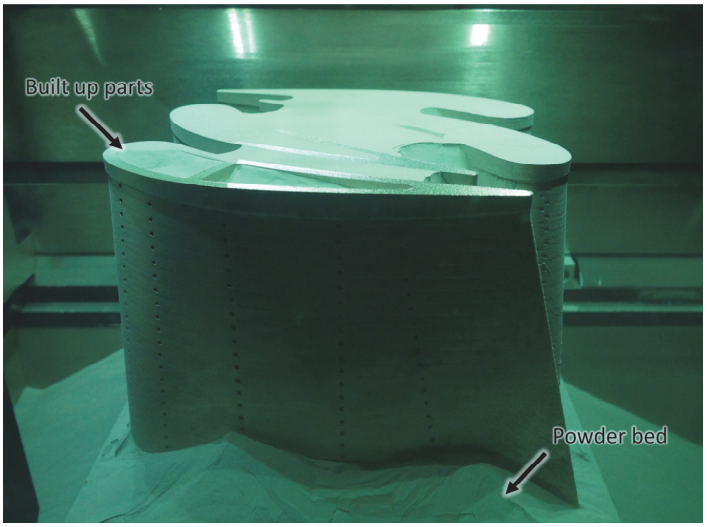

Figure 2: A completed LPBF build showing the built up parts partially raised out of the powder bed.

The LPBF process is usually performed with nitrogen or argon gas flowing over the powder bed with a high velocity, acting not only as an inert atmosphere but also as a fluid conveyor to remove smoke, spatter, and entrained powder particles from the path of the laser beam. Note that the LPBF process is often called by other names: according to ISO/ASTM 52900:2021 the process is called Powder Bed Fusion – Laser Beam (PBF-

LB), but it is also sometimes referred to as Laser Beam Melting (LBM), Selective Laser Melting (SLM), Direct Metal Laser Solidification (DMLS), Direct Metal Laser Melting (DMLM), or Laser Cusing. LPBF is the most widely used acronym and so will be used in this text.

2.1.2. Powder feedstock

Metal powder used for LPBF processes is usually manufactured by means of gas atomization (GA) [2,3]. Typically, such powder has high sphericity and good flowability, as well as good packing density in the powder bed. Typical feedstock particle sizes vary between 10 and 60 µm, with a normal distribution. For alloys with complex compositions and significant content of oxidation prone elements like Al or Ti, the powder is manufactured by means of the Vacuum Inert Melting Gas Atomization (VIGA) process, whereby the constituent alloying elements are melted together under vacuum before being poured into an atomizer. An example of VIGA powder is shown in Figure 3.

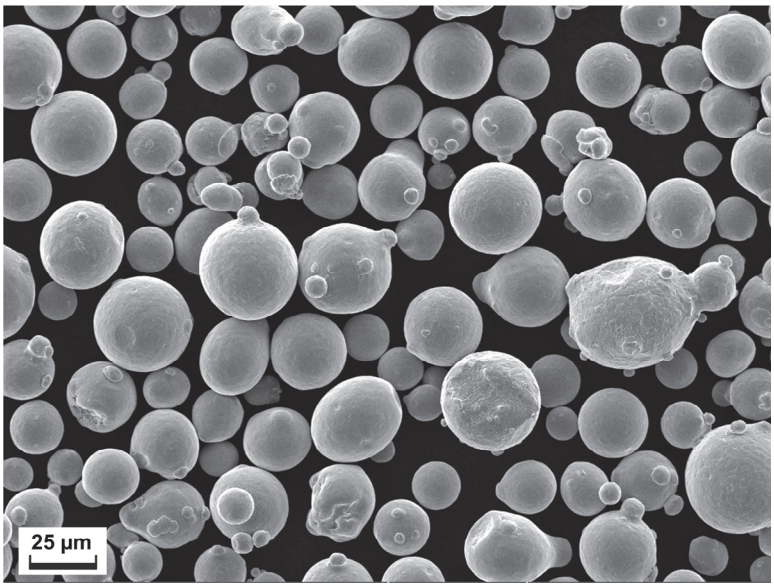

Figure 3: Typical IN625 VIGA powder for LPBF.

In general, powder manufactured by more specialized atomization technologies are more costly. For example, VIGA powder is more expensive than GA powder melted under inert gas, which is more expensive than water-atomized powder [2]. The use of GA or VIGA powder variants adds to the high cost of components manufactured by LPBF. Note that water-atomized powder has also successfully been used in LPBF, and depending on the powder handling, LPBF system hardware, and component application requirements, cheaper raw material such as water-atomized powder is not inherently unsuitable [4]. In some cases (especially for

alloys of Ti) powder used for LPBF is produced by using highly specialized plasma atomization or Plasma Rotating Electrode Process (PREP) atomization. These processes make almost perfectly spherical powder with very tightly controlled composition, but at a premium price compared to GA methods. A comprehensive overview of these atomization technologies is given elsewhere [2,4].

2.1.3. Process parameters

Compared to other metal AM manufacturing processes, LPBF manufactured parts typically have an excellent combination of low porosity, good mechanical properties, productivity, feature resolution, and surface finish [3,5]. Particularly with regards to density and mechanical performance of parts, LPBF has the advantage over most other processes. However, achieving low porosity and good mechanical properties in LPBF parts requires development and control of several process parameters.

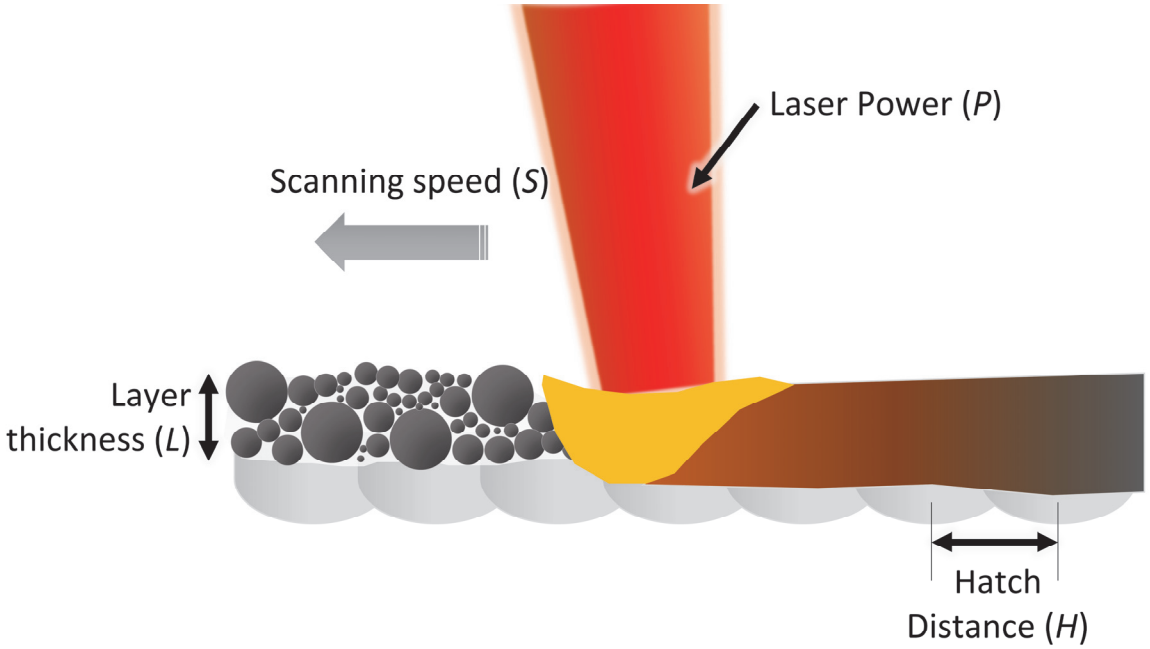

Figure 4: The primary parameters of the LPBF process.

While there are numerous parameters controlling various aspects of the LPBF process, the main process parameters which must be optimized to achieve highly dense material are shown in Figure 4.

LPBF consolidates powder by melting it in a pattern of lines called melt tracks. The spacing between adjacent melt tracks must be narrow enough to ensure overlap and fusion. Melt tracks must also be deep enough to penetrate down to the previous layer, or even remelt the underlying layer (or multiple layers). The laser power (P) is an important parameter which determines the width and depth of a melt track. The scanning speed (S) has a major effect as well. Faster scanning generally results in narrower and shallower melt tracks. The hatch distance (H) is the distance between two adjacent melt tracks. The layer thickness (L) determines the volume of material that must be melted in each layer, and this parameter also impacts the feature resolution of the process. A combined value to represent a combination of these parameters is often used, and this is called the Volumetric Energy Density, or E_v, which is expressed in J/mm^3 as follows:

$$E_V = \frac{P}{L \,.\, H \,.\, S}$$

A hardware parameter affecting the feature resolution is the spot size of the laser beam. A small spot size allows finer details to be printed, while a larger spot size allows faster consolidation of material.

The combination of above mentioned process parameters and their sequence during scanning of the component cross-section is the scanning strategy. The scanning strategy refers to the pattern of vectors traversed by the laser spot in order to eventually melt a whole layer. The scanning strategy may stay the same for every layer, or it may change from one layer to the next. This set of parameters has a major impact on development of microstructure, texture, and hence resulting mechanical properties in a component. Scanning strategy complexity and effects on 316L mechanical properties have been discussed extensively by Leicht [6].

2.1.4. Material properties

Alloys manufactured by LPBF typically have smaller grain size than cast or wrought materials. The large residual stress in the material immediately after the process results in a high dislocation density in the microstructure. This leads to a notable strain hardening effect, and higher yield strengths at ambient temperature compared to conventionally manufactured material. LPBF materials typically also exhibit anisotropy, meaning that properties parallel to the building direction (BD, the direction along which layers are added) are different compared to properties perpendicular to the building direction. Grains are typically long and columnar parallel to the BD, leading to somewhat lower strength and higher ductility in this orientation compared to properties perpendicular to the BD [5,7].

2.1.5. Defects

As with most other powder metallurgy (PM) processes, LPBF is also susceptible to residual porosity and other defects that form during consolidation. Some typical defects are shown in Figure 5. The most common defects are Lack of Fusion (LoF) defects and gas porosity. LoFs form between layers or between melt tracks. These can occur when there is not enough energy to fully melt the required volume of powder, or the melt is not fluid enough to flow into the empty space. LoF porosity is usually very irregular in shape. Gas porosity can form from entrapped or evolved gas in the melt pool, and typically looks very spherical.

Another type of porosity found in LPBF parts is keyhole porosity, which can form when there is excessive energy in a melt pool resulting in vaporization of material and formation of a round void at the bottom of the melt track.

Crack formation can also occur in LPBF parts, but typically is found only in alloys with complex compositions, e.g. Al- or Ni-base alloys, or alloys which solidify with high residual stress in a brittle microstructure, such as high carbon steels or alloy steels.

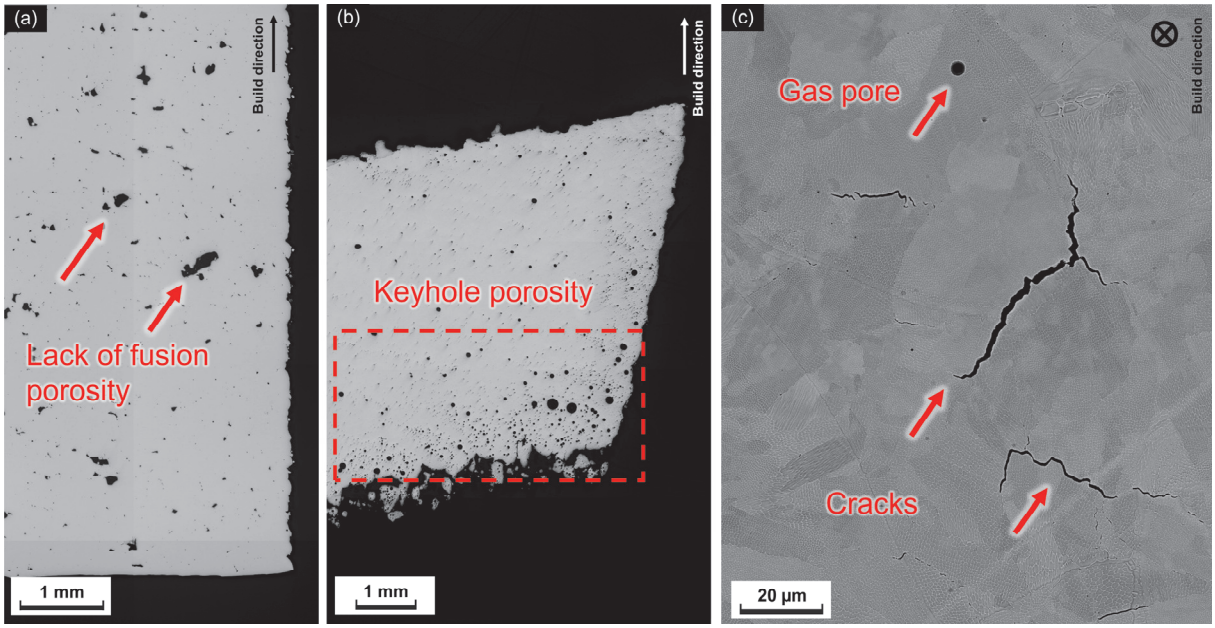

Figure 5: Several common defects that may be encountrered in LPBF processed parts: (a) Lack of fusion porosity; (b) Keyhole porosity; (c) cracks and gas porosity.

2.1.6. Heat treatments and HIP

Different alloy systems require different heat treatments. However, most LPBF produced parts require at least a stress relief heat treatment before they are separated from the building platform. This is in order to avoid deformation of the part due to the high residual stress in the as-built condition once the building platform constraint is removed. Additional heat treatments, such as homogenization, solution, ageing, etc. may be needed as per the requirements of the alloy system and/or application.

Hot isostatic pressing (HIP) is often used in high performance LPBF parts to minimize residual defects, especially in the medical and aerospace industries. HIP works by exposing the components to a high temperature and simultaneously a very high gas pressure (100 MPa or more) which is applied uniformly in all directions. This results in small scale plastic deformation and closure of defects. HIP can also be combined with other heat treatments to reduce the total number of operations in the manufacturing process chain.

The unique microstructure of LPBF manufactured parts means that heat treatments designed for cast or wrought alloys are not always suitable for LPBF alloys. Redevelopment of HIP or heat treatment regimes may therefore be needed in order to reach the desired properties in LPBF materials.

2.2. Metallurgy of Superalloys

Superalloys constitute a group of materials that are unique due to their combination of high strength, high corrosion and oxidation resistance, and the ability to demonstrate these characteristics at high temperatures. For this reason, superalloys have remained the materials of choice in many high temperature applications, especially in gas turbines for propulsion and power generation. Superalloys for use in the most demanding creep conditions are often directionally solidified (columnar grained) or even single crystal, but for the purpose of this review the focus will be on polycrystalline superalloys.

2.2.1. Strengthening mechanisms

Superalloys use Ni, Co, or a combination of Ni plus Fe as their base element. In all cases the alloy has an FCC crystal structure (γ phase) which is a tough and ductile starting point for alloying. The γ base is also stable to the solidus temperature, can dissolve many other alloying elements, and forms suitable oxides when alloyed with Cr and Al. This enables strengthening through a number of mechanisms, including solid solution strengthening, precipitation strengthening, and dispersion strengthening. Grain size strengthening has limited applicability in superalloys due to the high temperature nature of their service conditions, where grain size strengthening is no longer effective [8].

Solid solution strengthening plays an important role in most superalloys, as pure Ni has a low yield strength of only around 110 MPa at ambient temperature. Many superalloys feature additions of significant amounts of elements with large atomic radius differences to the base element (Ni, Fe, or Co) for solid solution strengthening. Elements having the largest solid solution strengthening effect are Al, W, Mo, and Cr. Many alloys that are intended primarily for oxidation or corrosion resistance applications tend to be strengthened by mainly solid solution strengthening elements. Solid solution strengthening is a useful strengthening mechanism as it remains in place even at high temperatures. However, some of the elements which contribute the most to solid solution strengthening also increase the propensity of formation of deleterious topologically close packed (TCP) phases after extended high temperature exposure. Mo and W in particular are also known to have harmful effects on hot corrosion resistance [9].

The high temperature strength and creep resistance for which modern Ni-base superalloys are well known is largely a result of large volume fractions of strengthening precipitates. Precipitates like γ' in Ni-base and γ'' in Ni-Fe-base superalloys are thermodynamically stable phases, which are precipitated out from super saturated solid solution using ageing heat treatments. The γ' phase is an ordered intermetallic phase with the formula A_3B, where A is Ni or Co and B is Al, Ti, Ta, or Nb. γ' has an L_{12} crystal structure and is coherent with the γ matrix. In basic terms, strengthening is a result of increased energy needed by dislocations to move through the ordered precipitate. The extent of strengthening from precipitates depends on the particle size of the precipitates, the volume fraction of the precipitates, coherency strains (difference in lattice parameters) between the γ matrix and γ' precipitate, and anti-phase boundary (APB) energy in the presence of the ordered precipitate. The strengthening effects of a precipitate are limited by the solvus temperature of the precipitate [8,9].

Dispersion strengthening by carbides and oxides are also commonly employed in superalloys. Dispersoids like carbides are incoherent with the γ matrix and are typically found at the grain boundaries in cast and wrought Ni-base superalloys. In discrete and blocky morphologies they provide a stabilizing effect at the grain boundary and have a favourable effect on creep resistance and strength. Carbides may also be found within grains, where they can act as barriers to dislocation movement in similar ways as precipitates. [8,9]

Oxide dispersion strengthened (ODS) superalloys are sometimes considered as a separate class of superalloys as they are manufactured by PM processes. They contain about 1 wt.% of nano-sized oxides, such as yttria Y_2O_3, mechanically alloyed during the manufacturing process. These incoherent oxides are stable to very high temperatures (above the melting point of the alloy) and this allows the alloys to have good creep resistance

and strength at very high temperatures (> 900°C) though intermediate temperature (600°C to 800°C) strength is low compared to conventional precipitation strengthened Ni-base superalloys [8,9].

Note that the strengthening mechanisms described above are often found together in a single alloy where their effects are superimposed.

2.2.2. Alloying elements and their effect on microstructure and properties

Superalloys are some of the most complex alloys ever designed in terms of their compositions, often having more than ten elements as alloying additions. Each alloying element can have multiple effects, and the extent of these effects can also be dependent on other alloying elements, as well as the manufacturing method of the alloy and its intended application. Some of the main roles played by major alloying elements in polycrystalline Ni-base superalloys are described in this section.

Chromium is found in significant quantities in almost all superalloys, and it acts as a potent solid solution strengthening element, but also as an oxide former. Chromia, Cr_2O_3, forms very fast in Cr-rich superalloys and provides very strong protection against hot corrosion. Cr in excessive amounts can result in formation of TCP phases after extended high temperature exposure, which reduce alloy strength and ductility [8,9].

Aluminium is alloyed in superalloys in smaller amounts than Cr but has important implications for both surface oxide stability and mechanical properties. In aged condition it forms γ' which provides precipitation strengthening, while in solid solution it contributes to solid solution strengthening. Al also forms alumina, Al_2O_3, which is more stable at higher temperatures than Cr_2O_3 and thus provides a higher level of oxidation protection. As a rule of thumb, a Cr to Al ratio of 4 or less is needed for an alloy to be an alumina rather than chromia former [8,9].

Cobalt is often added to Ni-base alloys in large quantities, as it raises the solidus temperature of the alloy, and can also increase the volume fraction and stability of γ', adding to strength [8,9].

Titanium like aluminium increases the volume fraction of γ' phase and also raises its solvus temperature. Further, Al increases the APB energy and adds to strengthening. Titanium is also a strong carbide former, and during solidification it will segregate to the liquid along with carbon, eventually forming carbides of the MX type in the inter-dendritic regions upon solidification [9].

Tantalum and niobium play a very similar role in Ni-base superalloys. Although they have very large misfit with the γ lattice, their solid solution strengthening effect is not great because they partition heavily to γ' phase or are trapped in stable MX type carbides. Both these elements increase γ' volume fraction. Tantalum has a

very high density and cost, so often Nb is preferred as an alloying element, especially in more cost sensitive applications [9].

Tungsten and molybdenum are both heavy refractory elements that have a strong solid solution strengthening effect in Ni-base superalloys. These elements also reduce overall diffusivity in the γ matrix and can lead to increased stability of carbide and γ' phases, and hence slowdown creep mechanisms. They also increase the solidus temperature of the alloy and solvus temperature of the γ' phase. On the other hand, both elements form unstable oxides, which can lead to poor hot corrosion performance. They can also form TCP phases after extended high temperature exposure, similar to Cr [8,9].

Other elements added purposefully to polycrystalline Ni-base superalloys include C, B, Zr, and Hf, which are all added in relatively small amounts but have major impacts on the properties of the alloys. These elements all have very limited solubility in the γ matrix and so segregate to the grain boundaries.

Carbon is added primarily for forming carbides, which strengthen the grain boundaries when in suitable morphologies and quantities. Carbon also refines the melt in liquid processing by de-oxidizing and de-sulfurizing, and makes the liquid metal more fluid. However, carbon also segregates heavily to the last liquid during solidification, and can contribute to poor weldability of many superalloys [8,9].

Boron is added to Ni-base superalloys only in amounts of less than 0,1 wt.%, but has a pronounced effect on creep strength. It has been found that B is essential for creep life and ductility, and the mechanism is thought to be that B inhibits grain boundary diffusion processes that lead to failure in creep. Boron is found in elemental form at grain boundaries when in low concentrations, but at higher concentrations it forms borides with elements like W, Mo, and Cr. Boron is also thought to inhibit carbide coarsening and grain growth. However, it can be detrimental for weldability and drastically lowers the incipient melting temperature of superalloys [8,9].

Zirconium is also considered important for creep property enhancement of Ni-base superalloys. It has been thought that Zr prevents grain boundary carbides from agglomerating, and thus prevents formation of microcracks at the grain boundaries. However, the importance of Zr has been questioned in recent decades and high creep strength alloys without Zr alloying have also been developed. Zr also has the effect of being a melting point depressant, and seems to have synergistic effects with B leading to poor welding [8,9].

Hafnium is not found as commonly in superalloys as B, C, or Zr, but is supposed to have similar positive effects at the grain boundaries. It changes the grain boundary γ' morphology and promotes eutectic γ/γ' formation, which can accommodate slip better than the regular γ' within grains. It also helps prevent carbide

coarsening similar to the effect of Zr. Note that Hf is the strongest carbide former of all alloying elements mentioned. Another effect of Hf is an increase in oxidation and sulfidation resistance [9].

2.2.3. Cracking mechanisms and cracking susceptibility

The thermal cycle of rapid heating and cooling during LPBF can be considered analogous to fusion welding, hence cracking mechanisms will be described using well-reported cracking susceptibility of the Ni-base superalloys during welding. The welding of superalloys is generally considered to be challenging, as these materials can be affected by several different types of cracking. Welding can also result in excessive segregation and formation of deleterious microstructures in the weld metal, which affect material performance. However, for the current discussion the issues around cracking are more relevant.

Solidification cracking is a common mechanism of cracking found in superalloys. Cracks occur in the fusion zone of the weld during solidification of the liquid weld metal. Cracks typically occur at grain boundaries, between two interfaces which are solidifying, due to a lack of liquid metal to fill the channel between the interfaces, and the opposing strains caused by contraction and cooling. Liquid stabilizing elements such as B, C, and Zr are often associated with this cracking mechanism. Solidification cracks typically have a tell-tale dendritic appearance [10].

Liquation cracking typically occurs in the heat affected zone (HAZ) of a weld, when low melting point phases, such as eutectics or borides melt at temperatures below the solidus temperature of the surrounding solid due to the heat from a weld pass. The residual stress in the weldment causes this liquified material to be pulled apart to form a crack [10].

Strain age cracking (SAC) is a cracking mechanism which affects mainly γ’ strengthened alloys. Unlike solidification and liquation cracking (referred to together as hot cracking) which occur during welding, SAC occurs during heating of the weldment after welding. When the material is heated to the ageing temperature, a sharp reduction of ductility caused by rapid precipitation of the γ’ phase, combined with pre-existing residual stress, causes the material to crack at grain boundaries. This type of cracking is why many high γ’ volume fraction superalloys are considered “difficult-to-weld” [10].

Ductility dip cracking (DDC) is another cracking mechanism often discussed in welding literature. This term simply refers to any cracking that occurs mainly due to exhaustion of ductility in or around a weld. In Ni-base alloys this is related to the phenomenon of Intermediate temperature embrittlement (ITE) whereby many alloys

suffer from extremely low ductility between approximately $0{,}5T_m$ and their solidus temperature [11]. A combination of this low ductility and very high residual stress from welding can often cause the material to crack without any other apparent cause [10].

2.2.4. Specific alloys studied

Two alloys were studied during the duration of this work: Haynes® 282® and Inconel 939. Both alloys are γ' strengthened superalloys and their compositions are given in Table 1. Compositions of other common superalloys discussed in the AM literature have also been given for comparison.

Inconel 939 (IN939) is a Ni-base superalloy that was developed in the late 1960s and 1970s for use in gas turbine hot sections. It is widely used in vanes / nozzles and ring segments / heat shields for many industrial gas turbines. IN939 is typically manufactured by vacuum induction melting and investment casting. IN939 has roughly 35 to 40% volume fraction of γ', and it also has significant alloying of Cr for good oxidation resistance [12,13]. IN939 is often regarded as difficult-to-weld, however reports suggest that its weldability is better than its predecessor alloys like IN738LC [13,14].

wt%	Cr	Co	Fe	W	Mo	Nb	Ta	Ti	Al	Zr	B	C	Ni	Others
Haynes® 282®	19	10	<1,5	<0,5	8,5			2,1	1,5	<0,02	0,0060	0,06	Bal	
IN939	22,5	19	-	2	-	1	1,4	3,7	1,9	0,1000	0,0100	0,15	Bal	-
IN738LC	16	8,5	-	2,6	1,75	0,85	1,75	3,4	3,4	0,0500	0,0100	0,11	Bal	-
IN718	19	<1	Bal (18,5)	-	3	5,1	-	0,9	0,5	-	< 0,0060	< 0,08	52,5	-
Hastelloy X	22	1,5	18,5	0,6	9	-	-	-	-	-	-	0,1	Bal	-
IN625	21,5	<1	<5		9	3,6	<0,05	<0,4	<0,4			<0,1	Bal	
CM247LC	8	9	-	10	0,5	-	3,2	0,7	5,6	0,0100	0,0150	0,07	Bal	1,4 Hf

Table 1: Nominal compositions of some superalloys discussed in the AM literature.

Haynes® 282® is a much newer alloy compared to IN939 and was patented as recently as 2005. It is mainly manufactured as a wrought alloy, and in conception was intended to have similar strength but better weldability than older wrought alloys like Waspaloy or René 41. As can be seen from the composition, it has lower nominal

amounts of C, B, and Zr than any of the aforementioned cast alloys. Haynes® 282® also has lower content of γ' forming elements, resulting in about 20% volume fraction of γ'. Instead, the alloy gains sufficient strengthening through solid solution strengthening as seen by the significant Mo alloying. Haynes® 282® has been shown to have excellent weldability especially in terms of SAC resistance [15].

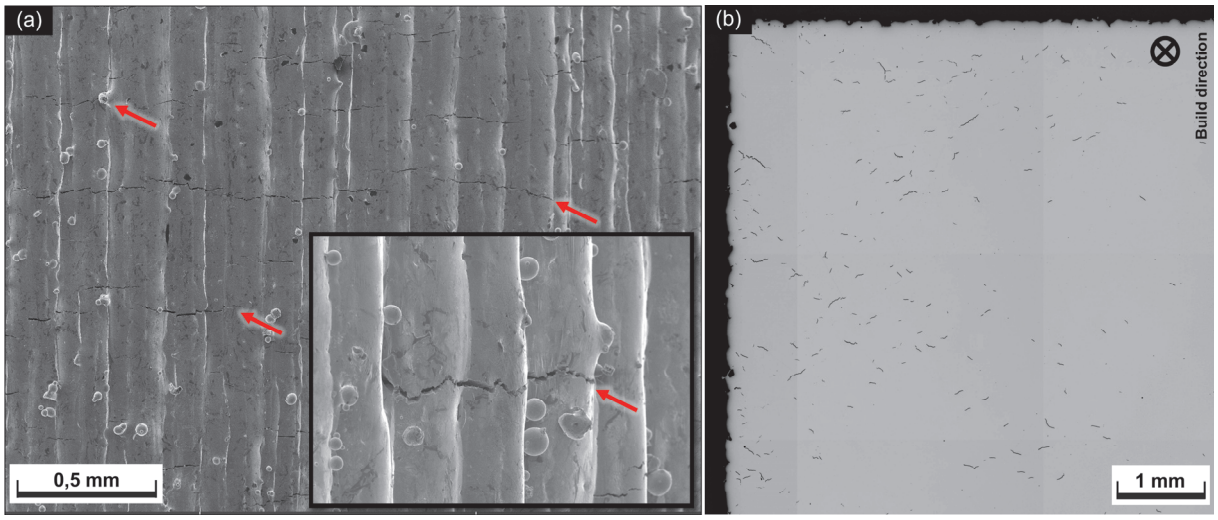

Figure 6: Microcracking in IN738LC produced by LPBF seen (a) direclty on as built surface by SEM, and (b) in polished cross-section by optical microscopy.

2.3. Challenges in LPBF of Superalloys

Although LPBF has seen industrial adoption by industries that make extensive use of superalloys, the variety of materials available for LPBF remains very limited. Weldable alloys like IN718 and IN625 remain the most common materials, and γ' strengthened superalloys are not commonly found in serial production applications. This is likely due to a number of challenges encountered when a superalloy is adopted or developed for LPBF.

2.3.1. Microcracking in LPBF processed Ni-base superalloys

The most common reported challenge in LPBF processing of superalloys is microcracking. This refers to small cracks, on the length scale of melt tracks, which form throughout the built material. It is clear that these defects are not acceptable in high performance materials, and would significantly degrade mechanical properties, especially fatigue properties, as they would act as initiation points for fracture. An example of microcracking is shown in Figure 6.

Microcracking has most commonly been associated with different forms of solidification cracking in the literature, largely due to the observation of dendritic morphology at the decohesion facets of cracks. Cracking has also been connected with grain boundary strengthening elements like B, Zr, C, and Hf, and their segregation, particularly at high angle grain boundaries.

Gruber et al. showed that variants of IN738 with both B and Zr produced the most microcracks in processing, while removing either one or both of these elements reduced the microcracking susceptibility. The study also showed the presence of B and Zr oxides on crack decohesion facets using specimens fractured in vacuum and analysed by advanced surface analysis techniques [16]. Kontis et al. also implicated B as the cause for cracking in a γ' strengthened superalloy processed in powder bed fusion - electron beam (PBF-EB), and claimed that liquation of Cr and Mo rich borides was the cause of cracking [17]. Chauvet et al. also observed B and borides at high angle grain boundaries which were correlated with cracks [18]. Hariharan et al. observed that in LPBF of IN738LC there was segregation of B and C to all grain boundaries, but Zr and Si only segregated to high angle grain boundaries. They further showed that an alloy with reduced levels of Si and Zr could be processed in LPBF with comparatively few cracks [19]. Zr segregation to grain boundaries was also the cited cause of solidification cracking according to Cloots et al. [20]. Vilanova et al. also showed that reduction of Zr and Si could improve the processability of IN738LC [21]. Another study by Engeli also pointed to excess Si as the cause of solidification cracking [22]. The negative effects of grain boundary strengthening elements on microcracking are fairly well established, however, these must be balanced with the positive effects of these elements on mechanical performance at high temperature. Després et al. further showed that removing Zr from the alloy AD730 could help overcome cracking, while maintaining acceptable creep performance. They also showed that removing both B and Zr had a drastically negative effect on creep performance [23]. Another grain boundary strengthening element, Hf, was removed from CM247LC by Griffiths et al., showing reduced microcracking susceptibility as a result [24]. On the other hand, mechanical blending of 1 to 2 wt.% Hf into prealloyed IN738LC powder by Yu et al. was claimed to have beneficial effects on cracking [25].

Apart from solidification and liquation cracking, other causes of microcracking have also been claimed in the literature. De Luca et al. atomized and printed a model alloy consisting of only Ni, Cr, Al and Ti, without any grain boundary strengthening elements, and found that the alloy still cracked due to solid state cracking, which they claimed to be a type of DDC [26]. Raza et al. explored the processability of IN713LC and claimed that cracking was caused by DDC, along with solidification cracking associated with Ti and Al segregation [27]. Tang et al. have also claimed some form of solid state cracking to be a mechanism in IN939 and CM247LC [28]. Catchpole-Smith et al. examined LPBF of CM247LC and presented DDC and liquation cracking as likely

causes [29]. An entirely different mechanism was reported by Qiu et al. for IN738LC whereby cracks were associated with Al, Si, and W oxide particles and their supposed embrittlement of grain boundaries [30].

Solid solution strengthened superalloys have also been associated with microcracking in LPBF, especially Hastelloy X. Tomus et al. showed that reduction in minor elements, especially C, eliminated the microcracking in Hastelloy X [31].

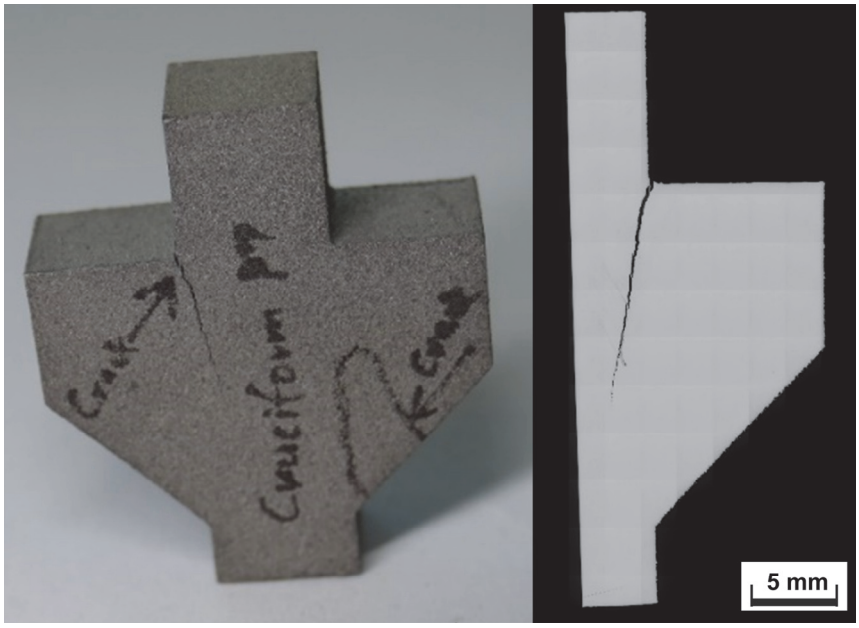

Figure 7: Post-process cracking in CM247LC produced by LPBF and subjected to heat treatment.

2.3.2. Post-process cracking

Unlike microcracking, post-process cracking usually occurs during heat treatment of the material after LPBF. Post-process cracking is most often associated with SAC, as cracks are often several millimeters in length and detectable in visual inspection. An example of post-process cracking is shown in Figure 7. Post-process cracking is not as extensively investigated as microcracking, but is perhaps a more severe problem from an industrial perspective. While microcracks can be healed by HIP processes, macrocracks formed in post-process are open to the surface and cannot be healed. Further, their large dimensions mean that they render affected

components largely useless. They are also more likely to occur in components with complex geometries, which nullifies one of the prime advantages of AM.

Post-process cracking has been found to occur mainly during the heat up phase of the stress relief or solution heat treatment, within the γ' precipitation temperature range. This is also the range where Ni-alloys suffer from intermediate temperature embrittlement [11]. Boswell et al. investigated the cause of post-process cracking in CM247LC and determined it to be a combination of SAC and DDC [32]. Hilal et al. also found severe macrocracking in CM247LC during HIP post-processing [33]. Post-process cracking in IN738LC was found by Gruber and Hallberg to occur during the heat up phase of heat treatment after LPBF, and it was shown that at least for simple geometries this could be solved using a HIP with a fast temperature ramp through the γ' precipitation temperature range [34,35]. Griffiths et al. observed that a Hf-free version of CM247LC showed reduced propensity for SAC, purportedly due to lower γ' precipitate volume fraction [36].

2.3.3. Specificity of AM microstructure

The properties of conventionally manufactured superalloys are often dependent on their processing history. For example, cast superalloys can have extremely large and non-uniform grain sizes, casting porosity, coarse carbides, and islands of γ and γ' eutectic. Wrought superalloys tend to have smaller more uniform grain size and fewer defects. These microstructure characteristics contribute to their performance in different applications. Therefore, achieving a crack-free superalloy build is not the final goal, but there is also the challenge of tailoring the microstructure to ensure performance.

A number of studies have indicated that the small grain sizes and columnar grains found in LPBF produced microstructures result in mechanical performance inferior in some aspects to cast or wrought levels. Significant anisotropy is also commonly observed between material built in varying orientations. Creep properties are especially affected, as grain boundaries are weak points in creep deformation. Rickenbacker et al. presented the high temperature mechanical performance of LPBF plus HIP processed IN738LC showing that the properties in the build direction are near the lower band of cast alloy performance, while the properties perpendicular to the build direction are significantly lower than cast. They suggested grain size as one of the probable causes, and suggested that special heat treatments need to be developed to improve the mechanical properties [37]. Similar conclusions were made by Wilkes et al. and Kunze et al. in a comparison of cast and LPBF IN738 alloys [38,39]. Geiger noted that the scanning strategy using the LPBF process could have a pronounced effect on texture, grain size and grain aspect ratio, and consequently mechanical performance and anisotropy [40]. Hilal et al. performed miniaturized creep testing of CM247LC produced by LPBF and observed severe anisotropy in creep performance [33]. High temperature performance of AM-produced René

65 was investigated by Wessman et al., and was found to be lacking compared to the wrought version of the alloy [41]. Even IN718 produced by LPBF has been shown to perform below the minimum requirement in stress rupture testing expected from the wrought alloy [42]. There have been few studies directly comparing cast or wrought alloys with AM counterparts, however one such study on LPBF and cast IN939 found that there were major differences in carbide morphology as well as minor differences in γ' volume fraction for similar heat treatment conditions. Bridges et al. performed extensive characterization of IN939 and found that while creep performance was lower than cast, LCF performance was as good or better than cast, and both effects were likely due to the smaller grain size of the LPBF material [43].

2.3.4. Heat treatment and post processing

As discussed above, the microstructure of LPBF processed superalloys is very different from that produced by conventional manufacturing processes. Since the typical solution and ageing heat treatments known in industry have been developed with conventionally manufactured microstructures as the starting point, it follows that solution and ageing heat treatments need to be re-evaluated or redesigned for LPBF starting microstructures. In several cases, where LPBF is not able to produce sufficiently defect-free microstructures, HIP may also be used to further densify the material.

Most studies performed on mechanical properties of LPBF processed crack susceptible alloys (e.g. IN738LC and CM247LC) have used HIP in order to heal cracks and other defects. However, HIP cannot heal all the defects, such as open to surface cracks or pores and removing large Ar-filled porosity is also challenging. Vilanova et al. studied the limits of defects that can be healed in IN738LC, and found that microcracks as large as 6 μm in width could be healed successfully [44].

Recrystallization heat treatments have successfully been used by several researchers to produce more equiaxed grain structures, larger grain sizes, and more isotropic properties in AM superalloys. Messé et al. showed that a low temperature stress relief before recrystallization could actually aid in producing more uniformly larger grains in LPBF produced IN738LC at lower temperatures [45]. Combinations of HIP and other heat treatment were required by Tomus et al. to successfully bring Hastelloy X mechanical properties to the level of the wrought material [46]. Pronounced reduction in anisotropy was also observed in the same material by Keshavarzkermani et al. after a static recrystallization heat treatment [47]. Boswell et al. and Christafidou et al. used recrystallization heat treatments in Haynes® 282® to enable isotropic high temperature performance in differently oriented samples [48,49]. These studies show that at least for some alloys there are real possibilities to optimize post processing to match the performance of cast and wrought materials while still retaining the benefits of AM.

Several strategies have been applied by researchers to overcome the challenges in LPBF processing of Ni-base superalloys discussed in the sections above. As described in preceding sections, several researchers have tried optimizing alloy compositions, especially regarding grain boundary strengthening elements, to overcome microcracking and post-process cracking issues [24,36]. There have also been several attempts at designing novel alloys optimized for AM, with varying levels of success [28,50–52]. Other strategies have included optimization of process parameters, e.g. by Perevoshchikova for IN738LC, or using pulsed / modulated lasers instead of continuous wave laser beams [53,54]. Addition of nucleating agent, e.g. ceramics like TiC has also been shown to be beneficial [55,56]. The intention of these strategies is to either promote faster solidification with less time for micro-segregation, or to promote solidification of small equiaxed grains which can accommodate stress without cracking. Strategies to reduce the residual stress generated during the process have also been demonstrated to be advantageous, such as high temperature processing of CM247LC by Hagedorn et al. [57]. Risse showed that using high temperature preheating could enhance the processability of IN738LC without formation of microcracks, while also promoting large grains beneficial for high temperature performance [53]. Gerstgrasser demonstrated the use of a second laser beam to reduce thermal gradient and residual stress in LPBF of CM247LC [58]. There also remain other performance critical issues, such as hot corrosion and oxidation performance, which are yet unknown for AM superalloys.

3. Materials and Methods

Details of experimental methods used in this thesis study have been described in detail in the individual appended papers. Below is given a general overview of the most relevant experimental techniques that were applied.

3.1. Powders

All powders used for LPBF processing were manufactured by the VIGA method, with predominantly spherical morphology and good flowability. Particle size distributions have been largely similar to the generic particle size distributions used for LPBF, i.e. between 15 to 45 μm. The individual chemical compositions of the powders, where relevant, e.g. in Paper II, are given in more detail.

3.2. LPBF systems and processing

All LPBF processing was performed on EOS M290 machines (Electro Optical Systems GmbH, Krailling, Germany), of which several different individual machines were used. The M290 has a 400W Yb fibre laser with a Gaussian intensity distribution and a spot diameter at focal plane of approximately 100 μm. The laser is mostly operated in continuous wave mode. This is representative of the most common LPBF processing conditions. In all experiments the machine was used with high purity Ar gas, and oxygen concentration below 0,1% in the process chamber. In general, process parameters used for the experiments were process parameter sets supplied by EOS for 40 μm layer thickness processing. For IN939 the process parameter set "EOS NickelAlloy IN939 PerformanceM291 1.00" was used, and for Haynes® 282® the process parameter set "EOS NickelAlloy HAYNES282 PerformanceM291 1.01" was used.

3.3. Heat treatment

After LPBF processing the printed samples were removed from the build plates by a bandsaw. Heat treatments were then performed in a TAV H4-S type industrial vacuum furnace (TAV Vacuum Furnaces SPA, Caravaggio BG, Italy) where Ar gas was used for the cooling phases of the cycle. N-type thermocouples were attached to dummy samples to accurately monitor the temperatures experienced by the parts inside the furnace.

3.4. Metallography

Samples for metallographic analysis were typically cut in either the XY plane or the ZY plane in order to observe the defects and microstructures. An explanation of the coordinate system and cutting directions is given in Figure 8. The samples were hot mounted in conductive Struers Polyfast resin (Struers ApS, Ballerup,

Denmark). The mounts were then progressively ground using SiC paper up to a P1000 paper. Fine grinding and polishing can be crucial steps in Ni-base alloys, as these materials are susceptible to smearing, which can hide defects, especially cracks. Fine grinding and polishing were done by using a woven cloth, Struers Mol with a 3 µm diamond suspension, followed by a Struers Nap with 1 µm diamond suspension. Depending on requirements further polishing with a Struers Chem cloth using 0,25 µm fumed silica suspension was also performed. Etching was typically performed electrolytically using 10% oxalic acid on a cotton swab with 3 to 6 V. In some cases immersion etching using Kallings II (waterless) reagent was also performed. Samples were typically ultrasonically washed and dried before microscopy.

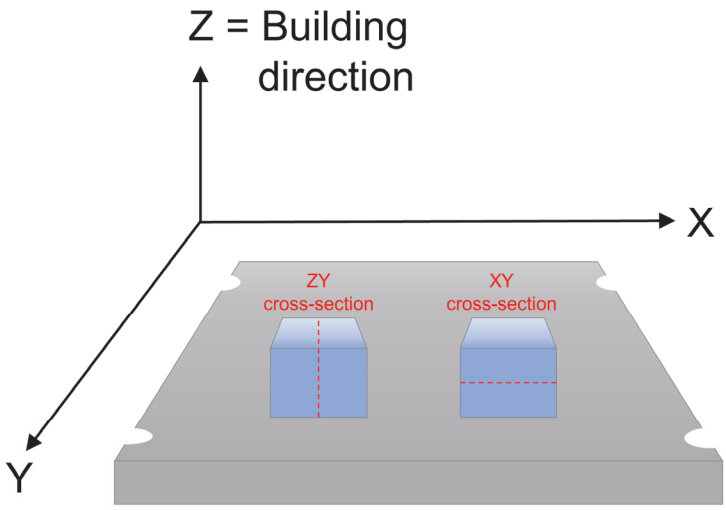

Figure 8: Coordinate system commonly used in LPBF builds, and cross-section orientations.

3.5. Microscopy

Optical microscopy was performed on an Olympus GX51 (Olympus Corporation, Nishishinjuku Shinjuku-Ku, Japan) inverted stage microscope. The microscope has a motorized stage that permits automated imaging and photography of large areas through stitching together of individual frames.

Electron microscopy was performed on a Zeiss Gemini SEM 450 (Carl Zeiss AG, Oberkochen, Germany) scanning electron microscope with a Field Emission Gun (FEG) electron source. The microscope has a number of detectors which were used for different purposes. The back-scattered electron (BSE) detector was used for

analysing chemical contrast, e.g. between matrix and carbides where carbides of high atomic number elements show lighter contrast compared to the matrix. The InLens detector of the microscope was also used extensively for higher magnification imaging, e.g. of fine γ' precipitates. This microscope is also equipped with two types of Energy Dispersive X-Ray Spectroscopy (EDX) detectors: a Bruker XFlash and a Bruker FlatQUAD (Bruker Corporation, Billerica, Massachusetts, US). The X-Flash was used for fast analysis of large features, e.g. compositional gradients in Paper II, while the Flat Quad was used mainly for mapping of fine features at high magnifications, e.g. carbides in Paper I. A Tescan Vega 3 SEM (Tescan Orsay Holding, a.s., Brno–Kohoutovice, Czechia) with a W-filament electron source was also used for fractography analysis.

3.6. Mechanical testing

All tensile and stress rupture testing performed for this work was conducted by accredited test laboratories. Machined specimens were used for testing. Tensile testing was typically conducted on cylindrical specimens with gauge lengths of around 25 mm and gauge diameters of 5 mm, similar to specimens described in the ISO 6892-1 tensile testing standard. Crosshead control mode was used with strain rates corresponding to 0,00025 s^{-1} until yield and 0,002 s^{-1} until fracture. For high temperature tensile testing the samples were allowed to stabilize at the target temperature for 30 minutes before testing was initiated. Samples for stress rupture testing were machined to 6 mm diameter with a 24 mm gauge length. Further details are mentioned in individual papers.

4. Summary of Results in Appended Papers

In this chapter the research questions defined in Section 1 are addressed by summarising the results from the appended papers.

RQ1 is addressed mainly by Paper I, as this paper was focused on evaluating the processability, microstructure, and mechanical performance of a weldable Ni-base superalloy. RQ2 is also addressed by this paper, since the results draw comparisons to the wrought microstructure of the studied alloy which is well known from the literature. RQ3 is the focus of Paper III and Paper IV, where investigation starts from the as-built microstructure and then explores the effects of solution and ageing treatments, with the objective of optimizing the heat treatment regime for the starting microstructure of the LPBF processed alloy. RQ3 is also the focus of Paper II from the perspective of the post-AM processing and for ensuring robustness in the process chain.

RQ 1: What are the main factors determining LPBF processability of weldable and non-weldable precipitation strengthened Ni-base superalloys?

The motivation behind **Paper I** was to perform a feasibility analysis of robust LPBF manufacturing of Haynes® 282®. As described in Section 2.2.4 above, Haynes® 282® is a relatively new superalloy, and was developed with the specific purpose of being weldable. It seemed that this would make it a perfect candidate for LPBF.

Evaluation of the processing window showed that the alloy does indeed exhibit excellent processability. Micrographs of LPBF processed Haynes® 282® are shown in Figure 9. Over the evaluated range of E_v it was found that LoF defects were formed below 45 J/mm^3, however no cracking could be observed even at high energy density parameters of up to 75 J/mm^3. Upon heat treatment, no macrocracks or other cracking was found, suggesting that despite high residual stress from the LPBF process, there is no strong tendency in Haynes® 282® towards SAC. This was found to be consistent with the welding literature.

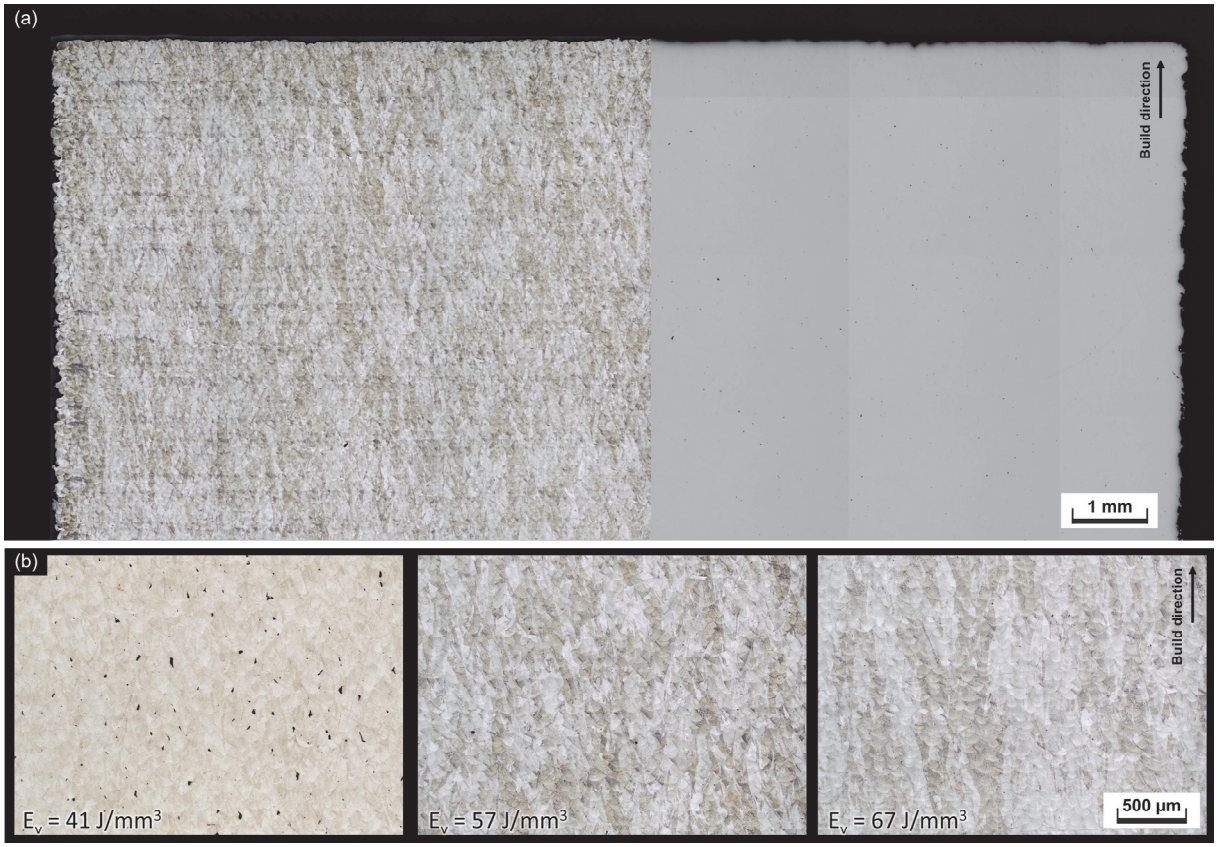

Figure 9: (a) Etched and plain polished cross-sections of LPBF processed Haynes® 282® in the as-built condition (b) microstructure produced with increasing E_v. No cracking was observed even at higher E_v.

With respect to RQ1, these results show that γ' precipitation strengthened superalloys can certainly be designed to be processable by LPBF, with regards to in-process cracking as well as post-process cracking. However, evaluation of more superalloys with varied compositions is required to better understand the aspect of processability, and to more comprehensively answer RQ1.

RQ 2: What are the main microstructural differences between conventional and LPBF processed Ni-base superalloys and their effect on mechanical performance?

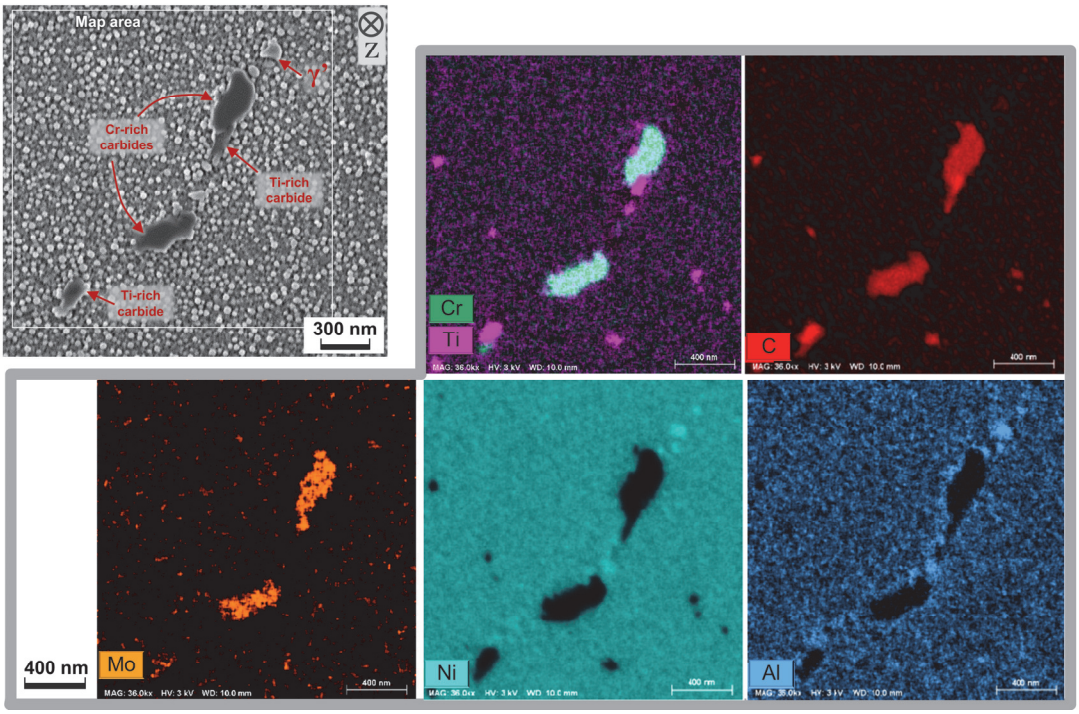

Figure 10: Grain boundary carbides observed in LPBF Haynes® 282®.

In the study of LPBF of Haynes® 282®, published as **Paper I**, the heat treatment approach used was to check feasibility of application of the standard heat treatment which is used for wrought Haynes® 282®. This heat treatment consisted of a solution treatment (1150°C / 2 hrs) and two ageing steps (1010°C / 2 hrs and 788°C / 8 hrs). It was found that no recrystallization occurred as a result of this heat treatment, and the columnar grain structure remained in place. However, dispersed carbides were observed to precipitate at the grain boundaries. EDX analysis showed that these carbides were Cr-rich $M_{23}C_6$ carbides or Mo-rich M_6C carbides – see Figure 10. Compared to the microstructure of the wrought material, which is well known from the literature, these carbides were very widely spaced and discontinuous at the grain boundaries. It was suggested that the reason behind this carbide distribution was the larger grain boundary surface area in the LPBF Haynes® 282®

compared to wrought. As the carbon content of the LPBF alloy was in the same range as commonly found in the alloy's wrought form, the carbon was spread over a much larger area, resulting in discontinuous carbides.

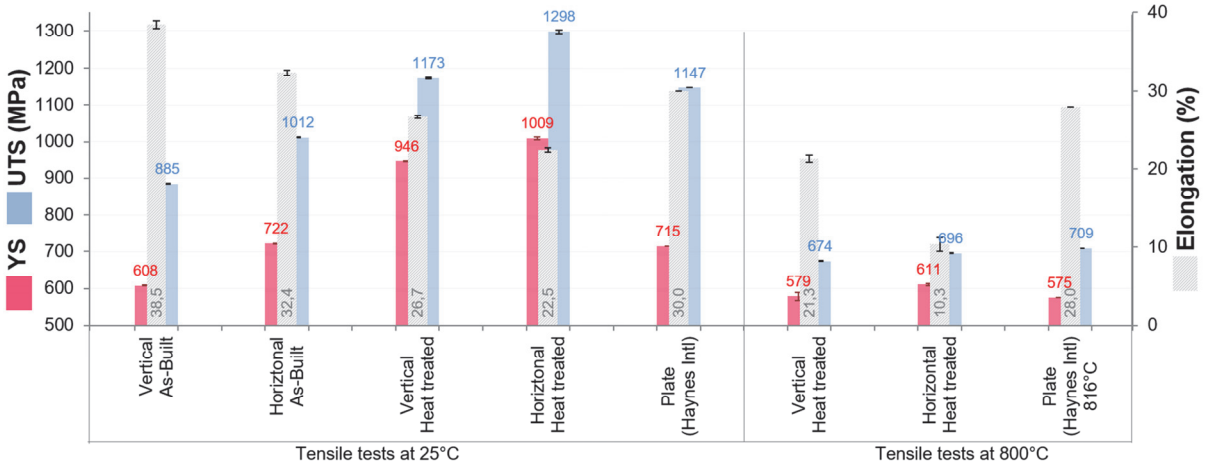

Figure 11: Room temperature and 800°C tensile results for LPBF Haynes® 282®.

The impact of the fine columnar grain structure was also observed in mechanical testing. Especially at room temperature in the as-built condition very high elongation values were observed. After ageing significant hardening was observed along with a drop in ductility. The LPBF material showed higher yield strength than known values of the wrought material, but also showed lower elongation. The elongation at higher temperatures was especially low, as shown in Figure 11. Anisotropy in the mechanical performance was also observed in the stress rupture testing results, where vertically built samples achieved almost three times the time-to-rupture value of the horizontally built samples. The horizontally built samples were unable to achieve the minimum stress rupture life required from the wrought material by relevant aerospace standards, while vertically built samples exceeded the requirement.

These results highlight several differences in microstructure and properties between LPBF processed and conventionally manufactured forms of the same alloy and are therefore considered relevant for RQ2.

RQ 3: What is the optimal post-AM heat treatment for LPBF produced precipitation-strengthened Ni-base superalloys?

One of the main challenges in enabling superalloys for LPBF is to reach the same level of performance expected of the respective alloys in their conventionally manufactured forms. As outlined in RQ3, this requires development of new heat treatment strategies, which, in turn, requires detailed understanding of the starting microstructure. This was the focus in **Paper III,** where the as-built microstructure of IN939 was studied in order to understand if and how the microstructure is different in phase constitution from the known as-cast microstructure, and how any existing differences may affect heat treatment options.

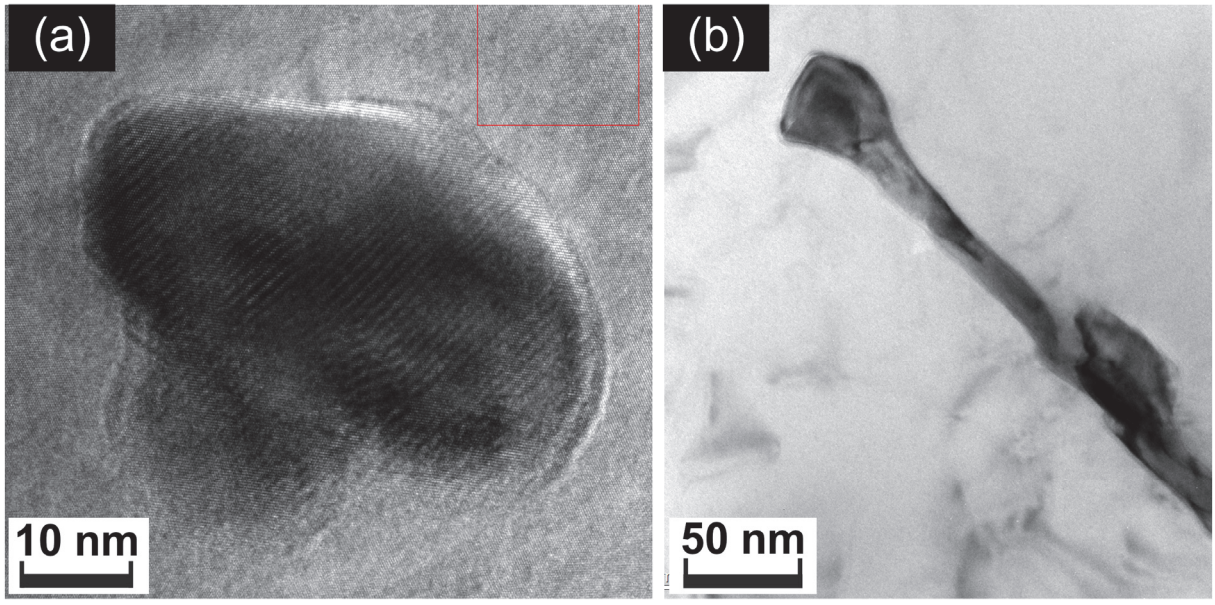

Figure 12: TEM observations of different particle morphologies at interdendritic regions of as-built LPBF IN939. (a) a carbide with blocky morphology; (b) Eta phase with acicular morphology.

Studies have shown that for several γ' strengthened superalloys processed by LPBF there are no precipitates of γ' in the as-built condition. This has led to the suggestion that it may be possible to omit the solution treatment from the heat treatment regime. However, the microstructure of IN939 in the as-cast condition contains the deleterious η phase as well, which can reduce alloy ductility if not dissolved by solution treatments. To understand the role of solution treatment in IN939, it was important to understand whether γ' and η phases were present in the as-built microstructure.

Analysis of the as-built microstructure of LPBF IN939 by TEM showed that there were several morphologies of phases present at the interdendritic regions. Small blocky particles were found to be MC carbides. Elongated

particles were also found, which through compositional analysis were understood to be η phase. Additionally, no γ' phase could be detected even in high resolution imaging. The two types of particles are shown in Figure 12.

The effect of ageing the microstructure with and without solution treatment was then tested. The material aged after solution treatment showed normal microstructure containing γ, γ', and carbide phases. The material aged without solution treatment showed precipitation of needle like η phase at the interdendritic regions. The effect of this microstructure was also seen by a drop in ductility in tensile testing. The two microstructures are compared in Figure 13. It was therefore established that for IN939 the solution treatment remains necessary, and while it does not act to solutionise γ', it does dissolve the η phase which is perhaps equally important. These results are significant with a view to RQ3, and they show that the post-AM heat treatment may need to be adapted depending on the phases observed in the as-built microstructure of any particular alloy.

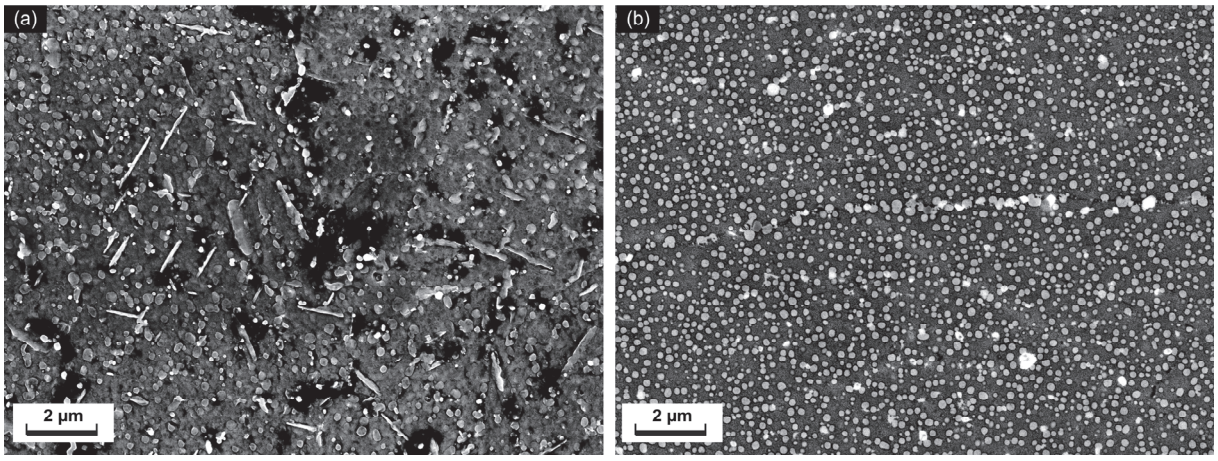

Figure 13: Microstructrue of LPBF IN939 (a) aged without solutionising, growth of Eta phase is apparent; (b) aged after solution treatment, showing only γ - γ' and carbides.

To further explore RQ3, the effect of an alternative ageing heat treatment on IN939 produced by LPBF was examined in **Paper IV**. The heat treatment most commonly utilized for IN939 consists of four steps, and totals 50 hours soaking time, which makes it time and cost intensive especially for a production scenario. Since IN939 in LPBF already has a different starting microstructure, the chance to re-develop the heat treatment represented an opportunity to make it more efficient as well. The alternative heat treatment consisted of 3 steps, totalling 14 hours soaking time. Characterization of samples from the old and alternative heat treatments showed that at room temperature and 600°C the new heat treatment produced more isotropic material with improved ductility. This was supposed to be related to the smaller and more dispersed carbides at grain boundaries.

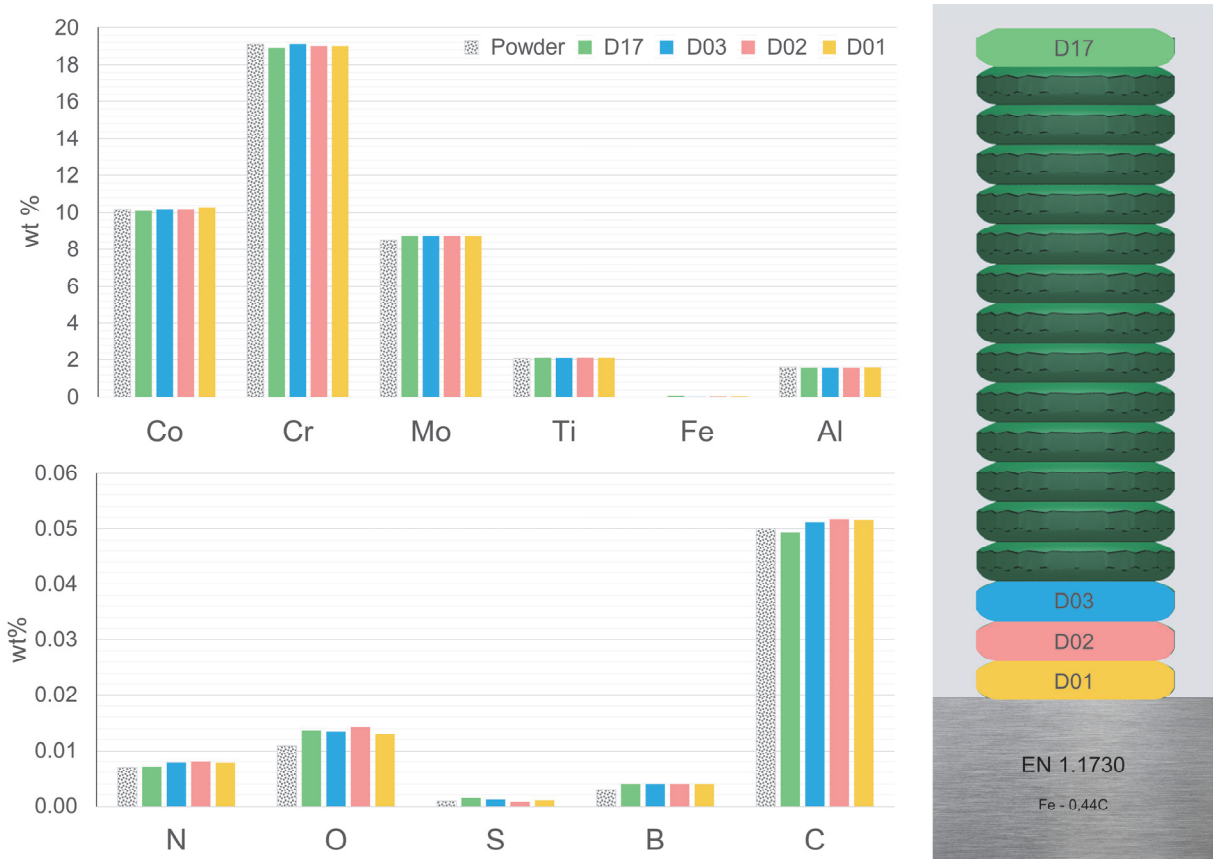

Figure 14: Chemical composition of LPBF Haynes® 282® at different build heights after heat treatment while attached to a steel platform, compared to the original powder composition.

RQ3 was also the focus of **Paper II**, designed as a model study to evaluate the effect of build platform on composition and properties of Ni-base superalloys during LPBF processing as well as post-AM heat treatment. This study intended to clarify doubts about contamination that may result in LPBF built material from use of dissimilar building platform (substrate) materials and on-platform heat treatment of parts. Paper II was initially intended as a side study, however, some aspects also deal with post-AM heat treatment and therefore address RQ3.

In many cases low alloy or carbon steels are used as building platform materials for LPBF of Ni-alloys. Steels are used because they are easy to machine and resurface, but mostly because they are economical. However, after printing of an LPBF part in an industrial manufacturing environment, the part undergoes a stress relief in order to relax the residual stresses from the LPBF process. This step is very important – if the part were to be

removed from the building platform without stress relief, it would distort and resultantly fail to be within the required dimensional tolerances of the 3D model. There is, however, a risk that the stress relief could induce diffusion of unwanted elements from the steel into the Ni alloy. It is known that performance of Ni alloys can be very sensitive to even ppm amounts of impurities. As no studies on this topic could be found, an experiment was designed to better understand the risk.

Samples of Haynes® 282® in the form of stacked discs were built on a 1.1730 steel building platform. The samples were then given a full solution and ageing heat treatment while still attached to the steel building platform. The discs, representing material at different build heights, were then separated and analysed for their chemical composition. The results (see Figure 14) showed that there was no major change in the bulk chemical composition of the Haynes® 282® compared to the powder used for printing. Importantly, there was no pickup of Fe, C, or S in the alloy. As the disk samples represented bulk material, and each disc was 3 mm in height, microanalysis using SEM and EDX was performed to understand the compositional gradient at a smaller scale. The results showed that there is indeed a compositional gradient at the build plate-component interface of around 200 μm where steel and Ni alloy are mixed. But this was not considered problematic as this mixed region was below the platform level, and also small enough to be removed by most cutting processes when the parts would be removed from the platform. This study, therefore, showed that using a steel building platform for LPBF of a Ni-base superalloy, even with on-platform heat treatment, does not jeopardise the robustness of the process chain.

With respect to RQ3, the results in this section highlight the importance of developing a detailed understanding of the as-built microstructure of LPBF superalloys in order to provide necessary input allowing to optimize heat treatments. The importance of solution treatments is especially stressed for the studied alloys.

5. Conclusions

With respect to the stated objective of evaluating the processability, microstructure, and properties of precipitation strengthened Ni-base superalloys by LPBF, and with attention to the specific research questions posed in Section 1, the following conclusions are made:

RQ 1: What are the main factors determining LPBF processability of weldable and non-weldable precipitation strengthened Ni-base superalloys?

In case of weldable Ni-base superalloys, studied in this work with the example of Haynes® 282®, characterised by a relatively low fraction of the γ' along with solid solution strengthening by Mo and a relatively high fraction of carbides, it was shown that this type of alloy has excellent processability by LPBF. Haynes® 282® could be manufactured without any form of cracking either during LPBF processing or during post-AM heat treatment.

RQ 2: What are the main microstructural differences between conventional and LPBF processed Ni-base superalloys and their effect on mechanical performance?

IN939 and Haynes® 282® Ni-base superalloys processed by LPBF, studied in this work, showed a columnar grain structure and a grain size that is much smaller than usually observed in wrought or cast alloys. This is seen to contribute to grain size strengthening effects and higher room temperature tensile strength than conventionally processed counterparts. Another major difference between LPBF and cast or wrought superalloys is grain boundary carbide morphology, however its effect on mechanical performance is not clear. The studied alloys, processed by LPBF, also displayed significant anisotropy in mechanical performance, especially respective to the LPBF building direction. The anisotropy is especially strong at high temperature, with material built perpendicular to the building direction showing limited tensile elongation and rupture life.

RQ 3: What is the optimal post-AM heat treatment for LPBF produced precipitation-strengthened Ni-base superalloys?

Detailed characterization of the as-built microstructure of IN939 showed that no γ' precipitation occurred during solidification of the material. However, the η phase with platelet morphology was found at interdendritic regions, and upon ageing was shown to grow rapidly and reduce the ductility of the alloy. These findings highlighted the essential role of solution treatment in the heat treatment regime, despite the absence

of γ'. Ageing treatment variations on LPBF IN939 showed that improvements in both, strength and ductility, could be achieved over the heat treatment used for cast IN939.

In an industrial manufacturing setting, post-AM heat treatment often starts with a stress relief heat treatment while parts are attached to the building platform. A risk of contamination during such heat treatment is seen to exist if the building platform has a different composition than the material being manufactured. A study of Haynes® 282® manufactured by LPBF and subsequently heat treated on a steel building platform showed that there was no large-scale change in chemical composition of the LPBF manufactured material. A region of compositional gradient between the steel and Haynes® 282® was identified, which was approximately 200 µm in width, and this was considered small enough as to be removed during cutting of the parts from the platform.

6. Future Work

The effect of minor alloying elements such as grain boundary strengtheners and their segregation upon solidification is especially important to explore for understanding of solidification cracking. In this respect, and to better answer RQ1, it is necessary to evaluate more superalloys with varied compositions, including various combinations and levels of grain boundary strengthening elements. A more extensive study of processability of a high strength non-weldable Ni-base superalloy was performed by the author, however the results are excluded from this thesis due to an on-going intellectual property protection process. The results are planned for publication during the continuation period of doctoral studies.

Manufacturing complex shapes through AM often involves building shapes with complex states of stress or stress raisers. This is known to lead to complications with post-process cracking, which is another aspect of processability and relevant to RQ1. For superalloys with higher fractions and faster precipitation of γ' it may be relevant to understand the effect of processing conditions, geometry, and heat treatment on post-process cracking.

For further work related to RQ2, a better understanding of microstructural and performance differences between LPBF and conventionally manufactured superalloys could be achieved by first hand testing under similar conditions, including high temperature tensile and creep testing followed by fractography and microstructure analysis.

With respect to RQ3, the existing work already shows that heat treatments have a pronounced effect on properties of LPBF superalloys, and the optimal heat treatment for a cast or wrought alloy is not necessarily well suited for a LPBF processed alloy. Redesigning heat treatments for alloys like Haynes® 282® is therefore an important area of opportunity for future work regarding RQ3. The target is to understand how the LPBF microstructure can be adapted to contribute to strengthening mechanisms, especially at high temperature. Specifically, it is interesting to understand the possibility to produce coarser grain structures in LPBF superalloys through homogenization, recrystallization and grain growth heat treatments.

7. References

[1] F42 Committee. Terminology for Additive Manufacturing - General Principles - Terminology: ISO/ASTM 52900:2021. West Conshohocken, PA: ASTM International.

[2] Hryha E, Riabov D. Metal Powder Production for Additive Manufacturing. In: Encyclopedia of Materials: Metals and Alloys; 2022; p. 264–271.

[3] Aumund-Kopp C, Riou A. Introduction to Additive Manufacturing Technology [Internet]. 3rd edn. Online; 2019. Available from: www.epma.com/am.

[4] Riabov D. The Effects of Morphology and Surface Oxidation of Stainless Steel Powder in Laser Based-Powder Bed Fusion [Licentiate Thesis]. Gothenburg, Sweden; 2020.

[5] DebRoy T, Wei HL, Zuback JS, et al. Additive manufacturing of metallic components – Process, structure and properties. Progress in Materials Science. 2018;92:112–224.

[6] Leicht A. Laser Powder Bed Fusion of 316L Stainless Steel: Microstructure and mechanical properties as a function of process parameters, design and productivity [Doctoral Thesis]. Gothenburg, Sweden: Chalmers University of Technology; 2020.

[7] Xu J, Gruber H, Boyd R, et al. On the strengthening and embrittlement mechanisms of an additively manufactured Nickel-base superalloy. Materialia. 2020;10:100657.

[8] Sims CT, Stoloff NS, Hagel WC. Superalloys II: High-Temperature Materials for Aerospace and Industrial Power. New York, USA: Wiley; 1987.

[9] Geddes B, Leon H, Huang X. Superalloys: Alloying and performance. Materials Park Ohio: ASM International; 2010.

[10] DuPont JN, Kiser SD, Lippold JC. Welding Metallurgy and Weldability of Nickel-base Alloys. Hoboken, New Jersey: John Wiley & Sons; 2009.

[11] Zheng L, Schmitz G, Meng Y, et al. Mechanism of Intermediate Temperature Embrittlement of Ni and Ni-based Superalloys. Critical Reviews in Solid State and Materials Sciences. 2012;37:181–214.

[12] Shaw SWK. Response of IN-939 to Process Variations. In: Superalloys 1980; 1980; p. 275–284.

[13] Gibbons TB, Stickler R. IN939: Metallurgy, Properties, and Performance. In: High Temperature Alloys for Gas Turbines 1982; 1982.

[14] G. Sjöberg, D. Imamovic, J. Gabel, O. Caballero, J.W. Brooks, J.-P. Ferté, and A. Lugan. Evaluation of the IN 939 Alloy for Large Aircraft Engine Structures. In: Superalloys 2004; 2004.

[15] Pike LM. Development of a Fabricable Gamma Prime Strengthened Superalloy. In: Roger C. Reed, Kenneth A. Green, Pierre Caron, et al., editors Superalloys 2008 (11th International Symposium); p. 191–200.

[16] Gruber H, Hryha E, Lindgren K, et al. The effect of boron and zirconium on the microcracking susceptibility of IN-738LC derivatives in laser powder bed fusion. Applied Surface Science. 2022;573:151541.

[17] Kontis P, Chauvet E, Peng Z, et al. Atomic-scale grain boundary engineering to overcome hot-cracking in additively-manufactured superalloys. Acta Materialia. 2019;177:209–221.

[18] Chauvet E, Kontis P, Jägle EA, et al. Hot cracking mechanism affecting a non-weldable Ni-based superalloy produced by selective electron Beam Melting. Acta Materialia. 2018;142:82–94.

[19] Hariharan A, Lu L, Risse J, et al. Misorientation-dependent solute enrichment at interfaces and its contribution to defect formation mechanisms during laser additive manufacturing of superalloys. Phys. Rev. Materials. 2019;3:44s.

[20] Cloots M, Uggowitzer PJ, Wegener K. Investigations on the microstructure and crack formation of IN738LC samples processed by selective laser melting using Gaussian and doughnut profiles. Mater. Des. 2016;89:770–784.

[21] Vilanova M, Taboada MC, Martinez-Amesti A, et al. Influence of Minor Alloying Element Additions on the Crack Susceptibility of a Nickel Based Superalloy Manufactured by LPBF. Materials. 2021;14:5702.

[22] Engeli R, Etter T, Hövel S, et al. Processability of different IN738LC powder batches by selective laser melting. J. Mater. Process. Technol. 2016;229:484–491.

[23] Després A, Antonov S, Mayer C, et al. On the role of boron, carbon and zirconium on hot cracking and creep resistance of an additively manufactured polycrystalline superalloy. Materialia. 2021;19:101193.

[24] Griffiths S, Ghasemi Tabasi H, Ivas T, et al. Combining alloy and process modification for micro-crack mitigation in an additively manufactured Ni-base superalloy. Additive Manufacturing. 2020;36:101443.

[25] Yu Z, Guo C, Han S, et al. The effect of Hf on solidification cracking inhibition of IN738LC processed by Selective Laser Melting. Materials Science and Engineering: A. 2021;804:140733.

[26] Luca A de, Kenel C, Griffiths S, et al. Microstructure and defects in a Ni-Cr-Al-Ti γ/γ' model superalloy processed by laser powder bed fusion. Materials & Design. 2021:109531.

[27] Raza M, Lo Y-L. Experimental investigation into microstructure, mechanical properties, and cracking mechanism of IN713LC processed by laser powder bed fusion. Materials Science and Engineering: A. 2021;819:141527.

[28] Tang YT, Panwisawas C, Ghoussoub JN, et al. Alloys-by-design: Application to new superalloys for additive manufacturing. Acta Materialia. 2021;202:417–436.

[29] Catchpole-Smith S, Aboulkhair N, Parry L, et al. Fractal scan strategies for selective laser melting of 'unweldable' nickel superalloys. Additive Manufacturing. 2017;15:113–122.

[30] Qiu C, Chen H, Liu Q, et al. On the solidification behaviour and cracking origin of a nickel-based superalloy during selective laser melting. Materials Characterization. 2019;148:330–344.

[31] Tomus D, Rometsch PA, Heilmaier M, et al. Effect of minor alloying elements on crack-formation characteristics of Hastelloy-X manufactured by selective laser melting. Additive Manufacturing. 2017;16:65–72.

[32] Boswell JH, Clark D, Li W, et al. Cracking during thermal post-processing of laser powder bed fabricated CM247LC Ni-superalloy. Materials & Design. 2019;174:107793.

[33] Hilal H, Lancaster R, Stapleton D, et al. Investigating the Influence of Process Parameters on the Structural Integrity of an Additively Manufactured Nickel-Based Superalloy. Metals. 2019;9:1191.

[34] Gruber H. Powder bed fusion processing of Ni-base superalloys: Defect formation and its mitigaton [Doctoral Thesis]. Gothenburg, Sweden: Chalmers University of Technology; September 2020.

[35] Hallberg E. Investigation of hot cracking in additive manufactured nickel-base superalloys - Emil Hallberg: Process optimization and crack removal with hot isostatic pressing [Masters Thesis]. Gothenburg, Sweden: Chalmers University of Technology; June 2018.

[36] Griffiths S, Ghasemi-Tabasi H, Luca A de, et al. Influence of Hf on the heat treatment response of additively manufactured Ni-base superalloy CM247LC. Materials Characterization. 2021;171:110815.

[37] Rickenbacher L, Etter T, Hövel S, et al. High temperature material properties of IN738LC processed by selective laser melting (SLM) technology. Rapid Prototyp. J. 2013;19:282–290.

[38] Wilkes J, Hoopes K, Helfand J. Creep and Tensile Properties of DMLS Inconel 738LC Coupons and Comparison to Cast Properties. In: The 6th International Supercritical CO2 Power Cycles Symposium; 2018.

[39] Kunze K, Etter T, Grässlin J, et al. Texture, anisotropy in microstructure and mechanical properties of IN738LC alloy processed by selective laser melting (SLM). Materials Science and Engineering: A. 2015;620:213–222.

[40] Geiger F, Kunze K, Etter T. Tailoring the texture of IN738LC processed by selective laser melting (SLM) by specific scanning strategies. Materials Science and Engineering: A. 2016;661:240–246.

[41] Wessman A, Cormier J, Hamon F, et al. Microstructure and Mechanical Properties of Additively Manufactured Rene 65. In: Tin S, Hardy M, Clews J, et al., editors Superalloys 2020; 2020; p. 961–971.

[42] Salam S, Mitama I, Sakata T. The Role of Microstructural Homogenization on Tensile and Stress-Rupture Behavior of Selective Laser Melted Nickel Based 718 Alloy. In: TMS 2020 149th Annual Meeting & Exhibition Supplemental Proceedings; 2020; p. 803–813.

[43] Bridges A, Shingledecker J, Torkaman A, et al. Metallurgical Evaluation of an Additively Manufactured Ni-Base Superalloy for Gas Tubrine Guide Vanes. In: Proceedings of ASME Turbo Expo 2020; 2020.

[44] Vilanova M, Garciandia F, Sainz S, et al. The limit of hot isostatic pressing for healing cracks present in an additively manufactured nickel superalloy. Journal of Materials Processing Technology. 2022;300:117398.

[45] Messé O, Muñoz-Moreno R, Illston T, et al. Metastable carbides and their impact on recrystallisation in IN738LC processed by selective laser melting. Additive Manufacturing. 2018;22:394–404.

[46] Tomus D, Tian Y, Rometsch PA, et al. Influence of post heat treatments on anisotropy of mechanical behaviour and microstructure of Hastelloy-X parts produced by selective laser melting. Materials Science and Engineering: A. 2016;667:42–53.

[47] Keshavarzkermani A, Esmaeilizadeh R, Enrique PD, et al. Static recrystallization impact on grain structure and mechanical properties of heat-treated Hastelloy X produced via laser powder-bed fusion. Materials Characterization. 2021;173:110969.

[48] Boswell J, Jones J, Barnard N, et al. The effects of energy density and heat treatment on the microstructure and mechanical properties of laser additive manufactured Haynes 282. Materials & Design. 2021;205:109725.

[49] Christofidou KA, Pang HT, Li W, et al. Microstructural Control and Optimization of Haynes 282 Manufactured Through Laser Powder Bed Fusion. In: Tin S, Hardy M, Clews J, et al., editors Superalloys 2020; 2020; p. 1014–1023.

[50] Xu J, Gruber H, Lin Peng R, et al. A Novel γ'-Strengthened Nickel-Based Superalloy for Laser Powder Bed Fusion. Materials (Basel). 2020;13. DOI: 10.3390/ma13214930.

[51] Zhou N, Dicus AD, Forsik SAJ, et al. Development of a New Alumina-Forming Crack-Resistant High-γ′ Fraction Ni-Base Superalloy for Additive Manufacturing. In: Tin S, Hardy M, Clews J, et al., editors Superalloys 2020; 2020; p. 1046–1054.

[52] Murray SP, Pusch KM, Polonsky AT, et al. A defect-resistant Co-Ni superalloy for 3D printing. Nat Commun. 2020;11:4975.

[53] Risse J. Additive Manufacturing of Nickel-Base Superalloy IN738LC by Laser Powder Bed Fusion [Doctoral Thesis, RWTH Aachen]. Aachen, Germany; April 2019.

[54] Guo C, Zhou Y, Li X, et al. A comparing study of defect generation in IN738LC superalloy fabricated by laser powder bed fusion: Continuous-wave mode versus pulsed-wave mode. Journal of Materials Science & Technology. 2021;90:45–57.

[55] Wei B, Liu Z, Cao B, et al. Cracking inhibition of nano-TiC reinforced René 104 superalloy fabricated by selective laser melting. Journal of Alloys and Compounds. 2021;881:160413.

[56] Zhou W, Zhu G, Wang R, et al. Inhibition of cracking by grain boundary modification in a non-weldable nickel-based superalloy processed by laser powder bed fusion. Materials Science and Engineering: A. 2020;791:139745.

[57] Hagedorn Y, Risse J, Meiners W, et al. Processing of nickel based superalloy MAR M-247 by means of High Temperature – Selective Laser Melting (HT – SLM). In: Bártolo PJ, editor Processing of nickel based superalloy MAR M-247 by means of High Temperature – Selective Laser Melting (HT – SLM): Advanced research in virtual and rapid prototyping ; proceedings of the 6th International Conference on Advanced Research and Rapid Prototyping, Leiria, Portugal, 1-5 October, 2013 ; [6th International Conference on Advanced Research in Virtual and Physical Prototyping (VR@P 2013); 2014; p. 291–295.

[58] Gerstgrasser M, Cloots M, Stirnimann J, et al. Residual stress reduction of LPBF-processed CM247LC samples via multi laser beam strategies. Int J Adv Manuf Technol. 2021. DOI: 10.1007/s00170-021-07083-6.